

Tensor-based Graph Learning with Consistency and Specificity for Multi-view Clustering

Long Shi, *Member, IEEE*, Lei Cao, Yunshan Ye, Yu Zhao, Badong Chen, *Senior Member, IEEE*

Abstract—In the context of multi-view clustering, graph learning is recognized as a crucial technique, which generally involves constructing an adaptive neighbor graph based on probabilistic neighbors, and then learning a consensus graph to for clustering. However, they are confronted with two limitations. Firstly, they often rely on Euclidean distance to measure similarity when constructing the adaptive neighbor graph, which proves inadequate in capturing the intrinsic structure among data points in practice. Secondly, most of these methods focus solely on consensus graph, ignoring unique information from each view. Although a few graph-based studies have considered using specific information as well, the modelling approach employed does not exclude the noise impact from the specific component. To this end, we propose a novel tensor-based multi-view graph learning framework that simultaneously considers consistency and specificity, while effectively eliminating the influence of noise. Specifically, we calculate similarity distance on the Stiefel manifold to preserve the intrinsic properties of data. By making an assumption that the learned neighbor graph of each view comprises a consistent part, a specific part, and a noise part, we formulate a new tensor-based target graph learning paradigm for noise-free graph fusion. Owing to the benefits of tensor singular value decomposition (t-SVD) in uncovering high-order correlations, this model is capable of achieving a complete understanding of the target graph. Furthermore, we derive an algorithm to address the optimization problem. Experiments on six datasets have demonstrated the superiority of our method. We have released the source code on <https://github.com/lshi91/CSTGL-Code>.

Index Terms—consistency, multi-view clustering, tensor-based graph learning, Stiefel manifold, specificity

I. INTRODUCTION

THE advent of the big data era has driven the prominence of multimedia data that originates from diverse sources [1]. For example, multimedia retrieval involves the integral utilization of color, textures, and edges [2], while video summarization requires the incorporation of multiple videos from distinct perspectives [3]. In the context of multimedia retrieval, each type of media data (color, textures, edges) can be considered as a different view. Consequently, multimedia

Long Shi, Lei Cao and Yu Zhao are with the School of Computing and Artificial Intelligence, and also with the Financial Intelligence and Financial Engineering Key Laboratory of Sichuan Province, Southwestern University of Finance and Economics, Chengdu 611130, China (e-mail: shilong@swufe.edu.cn, caolei2000@smail.swufe.edu.cn, zhaoyu@swufe.edu.cn), corresponding author: Long Shi

Yunshan Ye is with the School of Business Administration, Southwestern University of Finance and Economics, Chengdu 611130, China (e-mail: yeyunshan@sina.cn)

Badong Chen is with the Institute of Artificial Intelligence and Robotics, Xi'an Jiaotong University, Xi'an 710049, China (e-mail: chenbd@mail.xjtu.edu.cn)

The work of Long Shi was partially supported by the National Natural Science Foundation of China under Grant 62201475.

data can be treated as a representative class of multi-view data, which has found extensive applications in multi-view clustering [4], [5].

As a crucial unsupervised task, multi-view clustering overcomes the limitations of single-view clustering, particularly when the view is incomplete or the view data is noisy [6], [7]. In contrast to single-view clustering, a particular focus in multi-view clustering is on how to fuse data from multiple views to attain an enhanced data representation [8]. Multi-view Subspace Clustering (MVSC) aims to achieve a common subspace representation from multiple views, and then cluster a collection of data points based on the resulting low-dimensional subspaces [9]–[12]. To exploit both the low-rank and sparse properties of data, Brbić *et al.* [13] jointly enforced the associated constraints on the affinity matrix. In [14], the authors further investigated the l_0 quasi-norm-based regularization to address the overpenalized problem caused by l_1 -norm. Motivated by the underlying assumption that multiple views intrinsically originate from one shared latent representation, there has been an increasing interest towards the latent representation multi-view methods [15]–[17]. Luo *et al.* proposed an effective subspace learning framework that considers both consistent and specific representations [18]. More progress on multi-view subspace clustering methods can be found in [19]–[24].

Graph-based methods also hold an important standing in multi-view clustering. Nie *et al.* conducted several studies exploring the assignment of weights to different graphs for highlighting the significance of key views [25], [26]. Wang *et al.* [27] constructed a unified graph matrix which serves to fuse data graph matrices of all views. In [28], a parameter-free method that allows for structured graph learning was investigated. This method is also beneficial in reducing dimensionality. Liang *et al.* [29] formulated the consistent and inconsistent graph information in a unified optimization model. In [30], Kang *et al.* presented a graph learning framework that is able to preserve a complete structure of data. Li *et al.* proposed a consensus graph learning framework [31]. Wen *et al.* investigated the graph completion issue for incomplete views [32]. Further works related to graph-based methods are encouraged to refer [33], [34].

Recently, tensor-based methods have promoted the advancement of multi-view clustering towards the extraction of high-order data information [35]. Wu *et al.* [36] proposed an essential tensor learning method based on Markov chain for multi-view clustering. Considering that weakly supervised information can likely be acquired in real-world scenarios, Tang *et al.* [37] incorporated the weakly supervised infor-

mation when formulating the regularization constraints. By incorporating tensor with graph learning, several tensor based graph learning methods can be discovered in [38]–[41].

Most of the aforementioned graph-based methods can be considered as drawing inspiration from [26], [42]. In essence, these methods are variations of learning a consensus graph by fusing adaptive neighbor graphs from different views. Despite a few graph-based studies, such as [29], have attempt to consider both consistency and specificity, they model the similarity matrix with a consistent part and a specific part, without any further meticulous consideration. Specifically, they overlook the impact of noise, which could result in the specific information learned being contaminated with noise. To be more clear, these methods have the following limitations:

1) The adaptive neighbor graph is constructed using Euclidean distance, which probably fails to characterize the inherent properties of data.

2) Most methods do not consider view-specific information when learning the consensus graph. Although a few works have made preliminary explorations in this direction, the modeling approach does not exclude the influence of noise from the specific component. For more details, readers are encouraged to refer to the motivation subsection in Section III.

To address the drawbacks previously discussed, we propose a novel tensor-based graph learning framework, namely Tensor-based Graph Learning with Consistency and Specificity (CSTGL). We begin with learning the neighbor graphs of different views on the Stiefel manifold. The similarity between data points is measured using Stiefel distance. In contrast to Euclidean distance, Stiefel distance takes into account the orthogonal properties on the manifold [43], thereby providing a more accurate reflection of the underlying data structure. To facilitate the subsequent graph fusion, we make an assumption that the neighbor graph of each view can be explicitly modelled by a consistent component, a specific component, and a noise component. Then, we formulate a new tensor graph learning framework that takes full advantage of both consistent and specific information, while effectively mitigating the influence of noise. Our model can exploit the high-order correlations among graphs, thanks to tensor singular value decomposition (t-SVD) [44]. CSTGL can be treated as a noise-free graph fusion framework, and our main contributions include:

- We learn the neighbor graph for each view by measuring the similarity distance on the Stiefel manifold, which enables the exploitation of the data’s inherent structure properties.
- By assuming that the neighbor graph of each view is composed of a consistent component, a specific component, and a noise component, we construct a complete tensor graph fusion framework that explicitly incorporates both consistent and specific tensor graphs, while effectively minimizing the impact of noise.
- An iterative algorithm is derived for solving the optimization problem in CSTGL.

Experiments demonstrate that CSTGL outperforms some SOTA baselines. Moreover, ablation studies confirm the bene-

fits of using Stiefel manifold distance for similarity measurement, as well as the improvements gained from the integration of consistent and specific tensor graphs.

The remainder of this paper is organized as follows. Section 2 presents notations and preliminaries. Section 3 shows the detailed procedures of CSTGL. Section 4 carries out extensive experiments to validate CSTGL’s performance. We finally draw some conclusions in Section 5.

II. NOTATIONS AND PRELIMINARIES

In the following, we list the notations used in this paper and introduce some fundamental definitions related to tensor. Moreover, we briefly review some relevant works.

A. Notations

In this paper, we use bold fonts to denote vectors or matrices, and utilize calligraphic fonts to represent tensors. For convenience, we summarize the definitions of notations in Table I. For a 3-order tensor $\mathcal{A} \in \mathbb{R}^{n_1 \times n_2 \times n_3}$, $\mathcal{A}(i, :, :)$ denotes the i -th horizontal slice of \mathcal{A} , $\mathcal{A}(:, i, :)$ represents the i -th lateral slice of \mathcal{A} , and $\mathcal{A}(:, :, i)$ accounts for the i -th frontal slice of \mathcal{A} . Since the i -th frontal slice of \mathcal{A} is frequently used in the paper, we define $\mathbf{A}^{(i)} = \mathcal{A}(:, :, i)$. The symbol $\mathbf{A}_{(i)}$ represents the unfolding matrix along the i -th mode of \mathcal{A} . $\hat{\mathcal{A}} = \text{fft}(\mathcal{A}, [], 3)$ stands for the fast Fourier transformation (FFT) of \mathcal{A} along the 3rd dimension. $\Phi(\mathbf{A}^{(1)}, \dots, \mathbf{A}^{(i)})$ spans a tensor using $\mathbf{A}^{(1)}, \dots, \mathbf{A}^{(i)}$. The definitions of various norms can be found in the table below.

TABLE I: Definitions of notations

Notations	Description
$(\cdot)^T$	Transpose of a vector, a matrix or a tensor
$\text{tr}(\cdot)$	Trace of a matrix
$\ \cdot\ _2$	l_2 -norm of a vector
$a, \mathbf{a}, \mathbf{A}, \mathcal{A}$	a scale, a vector, a matrix, a tensor
$\mathcal{A}(i, :, :)$	i -th horizontal slice of \mathcal{A}
$\mathcal{A}(:, i, :)$	i -th lateral slice of \mathcal{A}
$\mathcal{A}(:, :, i)$	i -th frontal slice of \mathcal{A}
$\hat{\mathcal{A}} = \text{fft}(\mathcal{A}, [], 3)$	FFT of \mathcal{A} along the 3rd dimension
$\mathcal{A} = \text{ifft}(\hat{\mathcal{A}}, [], 3)$	Inverse FFT of $\hat{\mathcal{A}}$ along the 3rd dimension
$\mathbf{A}^{(i)}$	$\mathbf{A}^{(i)} = \mathcal{A}(:, :, i)$
$\hat{\mathbf{A}}^{(i)}$	$\hat{\mathbf{A}}^{(i)} = \hat{\mathcal{A}}(:, :, i)$
$\mathbf{A}_{(i)}$	Unfolding matrix along the i -th mode of \mathcal{A}
$\Phi(\mathbf{A}^{(1)}, \dots, \mathbf{A}^{(i)})$	Span a tensor \mathcal{A} using $\mathbf{A}^{(1)}, \dots, \mathbf{A}^{(i)}$
$\ \mathbf{A}\ _F$	F -norm of \mathbf{A} : $\ \mathbf{A}\ _F = \sqrt{\sum_{ij} A_{ij}^2}$
$\ \mathbf{A}\ _*$	Nuclear norm of \mathbf{A} : sum of singular values
$\ \mathbf{A}\ _{2,1}$	$l_{2,1}$ -norm of \mathbf{A} : $\ \mathbf{A}\ _{2,1} = \sum_i \ \mathbf{x}_i\ _2$
$\ \mathcal{A}\ _F$	F -norm of \mathcal{A} : $\ \mathcal{A}\ _F = \sqrt{\sum_{ijk} \mathcal{A}_{ijk} ^2}$
$\ \mathcal{A}\ _{\textcircled{t}}$	t -SVD based tensor nuclear norm of \mathcal{A}
$\ \mathcal{A}\ _{2,1}$	$l_{2,1}$ -norm of \mathcal{A} : $\ \mathcal{A}\ _{2,1} = \sum_{i,j} \ \mathcal{A}(i, j, :)\ _2$

B. Fundamental Concepts

To facilitate the understanding of tensor-related concepts, we introducing the following definitions [44]:

Definition 1 (t-Product): Consider two tensors $\mathcal{A} \in \mathbb{R}^{n_1 \times n_2 \times n_3}$ and $\mathcal{B} \in \mathbb{R}^{n_2 \times n_4 \times n_3}$, the t-product $\mathcal{A} * \mathcal{B}$ is given by

$$\mathcal{A} * \mathcal{B} = \text{fold}(\text{bcirc}(\mathcal{A})\text{bvec}(\mathcal{B})), \quad (1)$$

where $\text{bcirc}(\mathcal{A})$ and $\text{bvec}(\mathcal{B})$ denote the block circulant matrix and block vectorizing operations, respectively, defined by

$$\text{bcirc}(\mathcal{A}) = \begin{bmatrix} \mathcal{A}^{(1)} & \mathcal{A}^{(n_3)} & \cdots & \mathcal{A}^{(2)} \\ \mathcal{A}^{(2)} & \mathcal{A}^{(1)} & \cdots & \mathcal{A}^{(3)} \\ \vdots & \ddots & \ddots & \vdots \\ \mathcal{A}^{(n_3)} & \mathcal{A}^{(n_3-1)} & \cdots & \mathcal{A}^{(1)} \end{bmatrix}, \quad (2)$$

and

$$\text{bvec} = [\mathcal{A}^{(1)}; \mathcal{A}^{(2)}; \cdots; \mathcal{A}^{(n_3)}]. \quad (3)$$

Definition 2 (f-Diagonal Tensor): A tensor is called f-diagonal if every frontal slice forms a diagonal matrix.

Definition 3 (Orthogonal Tensor): For a orthogonal tensor $\mathcal{Q} \in \mathbb{R}^{n \times n \times n_3}$, it satisfies

$$\mathcal{Q}^T * \mathcal{Q} = \mathcal{Q} * \mathcal{Q}^T = \mathcal{I}, \quad (4)$$

where \mathcal{I} represents the identity tensor with its frontal slice being a $n \times n$ identify matrix.

Definition 4 (t-SVD): For a tensor $\mathcal{A} \in \mathbb{R}^{n_1 \times n_2 \times n_3}$, one can factorize it by t-SVD as

$$\mathcal{A} = \mathcal{U} * \mathcal{G} * \mathcal{V}^T, \quad (5)$$

where $\mathcal{U} \in \mathbb{R}^{n_1 \times n_1 \times n_3}$ and $\mathcal{V} \in \mathbb{R}^{n_2 \times n_2 \times n_3}$ are orthogonal, and $\mathcal{G} \in \mathbb{R}^{n_1 \times n_2 \times n_3}$ is f-diagonal.

Definition 5 (t-SVD Based Tensor Nuclear Norm): The t-SVD based tensor nuclear norm of \mathcal{A} is defined by

$$\|\mathcal{A}\|_{\otimes} = \sum_{i=1}^{n_3} \|\hat{\mathcal{A}}^{(i)}\|_* = \sum_{j=1}^{\min(n_1, n_2)} \sum_{i=1}^{n_3} |\hat{\mathcal{G}}(j, j)|, \quad (6)$$

where $\hat{\mathcal{G}}^{(i)}$ is calculated by applying the SVD of frontal slices of $\hat{\mathcal{A}}$, i.e., $\hat{\mathcal{A}}^{(i)} = \hat{\mathcal{U}}^{(i)} \hat{\mathcal{G}}^{(i)} \hat{\mathcal{V}}^{(i)T}$.

C. Related Work

Before further proceeding, it is necessary to review two fundamental multi-view methods respectively corresponding to graph-based learning and tensor-based learning, namely Parameter-weighted Multiview Clustering (PwMC) [26] and t-SVD Multi-view Clustering (t-SVD-MSC) [35].

1) *PwMC*: Suppose we need to partition n samples into c clusters, for given similarity matrices $\mathbf{A}^{(v)} \in \mathbb{R}^{n \times n}$ from different views, PwMC learns the target graph \mathbf{S} by solving the following objective function

$$\begin{aligned} \min_{\alpha^{(v)}, \mathbf{S}} \sum_{v=1}^m \alpha^{(v)} \|\mathbf{S} - \mathbf{A}^{(v)}\|_F^2 + \gamma \|\alpha\|_2^2 \\ \text{s.t. } \alpha^{(v)} \geq 0, \alpha^T \mathbf{1} = 1, s_{ij} \geq 0, \mathbf{s}_i \mathbf{1} = 1, \\ \text{rank}(\mathbf{L}_s) = n - c \end{aligned} \quad (7)$$

where m denotes the number of views, $\alpha = [\alpha^{(1)}, \alpha^{(2)}, \dots, \alpha^{(m)}]$, $\gamma > 0$, and $\text{rank}(\mathbf{L}_s)$ represents the rank of the Laplacian matrix \mathbf{L}_s . The Laplacian matrix is defined as $\mathbf{L}_s = \mathbf{D}_s - (\mathbf{S}^T + \mathbf{S})/2$, where $\mathbf{D}_s \in \mathbb{R}^{n \times n}$ denotes the degree matrix, which is diagonal, with the i -th diagonal element determined by $\sum_j (s_{ij} + s_{ji})/2$. Inspired by the idea of learning the target graph in PwMC, many variants have been explored [31], [45], [46].

2) *t-SVD-MSC*: To capture the low rank tensor subspace and high-order correlations among views, t-SVD-MSC performs a rotation on the tensor and imposes a low-rank tensor constraint on the rotated tensor. Given a set of multi-view data matrices $\{\mathbf{X}^{(v)}\}_{v=1}^m$, with $\mathbf{X}^{(v)} \in \mathbb{R}^{d_v \times n}$ denoting the v -th view data with d_v dimensions, the objective function of t-SVD-MSC is defined as:

$$\begin{aligned} \min_{\mathbf{Z}^{(v)}, \mathbf{E}^{(v)}} \lambda \|\mathbf{E}\|_{2,1} + \|\mathcal{Z}\|_{\otimes}, \\ \text{s.t. } \mathbf{X}^{(v)} = \mathbf{X}^{(v)} \mathbf{Z}^{(v)} + \mathbf{E}^{(v)}, v = 1, \dots, V, \\ \mathcal{Z} = \varphi(\mathbf{Z}^{(1)}, \mathbf{Z}^{(2)}, \dots, \mathbf{Z}^{(V)}), \\ \mathbf{E} = [\mathbf{E}^{(1)}; \mathbf{E}^{(2)}; \dots; \mathbf{E}^{(V)}], \end{aligned} \quad (8)$$

where $\mathbf{Z}^{(v)} \in \mathbb{R}^{n \times n}$ stands for the v -th view representation matrix, $\mathbf{E}^{(v)}$ is the v -th view error matrix, the function $\varphi(\cdot)$ serves to span a 3-mode tensor by stacking various representation matrix, with its dimensionality rotated to $n \times m \times n$.

Owing to the superior properties of t-SVD, t-SVD-MSC is capable of exploiting the comprehensive information among all the views. Motivated by the t-SVD based tensor multi-rank constraint, several multi-view tensor learning methods have been investigated [36], [38], [47], [48].

III. PROPOSED METHODOLOGY

We will introduce CSTGL, offering a detailed presentation of its motivation, model formulation, optimization procedures and computational complexity analysis. The framework of CSTGL is shown in Fig. 1.

A. Motivation

Our proposed CSTGL is motivated by the following three observations from graph-based methods:

Observation 1: In order to reflect the similarity among data samples, a common strategy is to learn the adaptive neighbor graph for $\mathbf{A}^{(v)}$ [31], [39]. However, most methods construct the adaptive neighbor graph using Euclidean distance, which may not effectively uncover the inherent structure of complex data.

Observation 2: We also notice that the majority of graph-based multi-view methods follow the learning scheme in (7) to attain a target graph from multiple views. Essentially, these methods focus on constructing a consensus graph by minimizing the discrepancy between the similarity graph and the target graph. This learning strategy notably emphasizes the importance of consistency among views. However, from another perspective, it seems to neglect the diversity inherent in different views.

Observation 3: Despite a few graph-based works, such as [29], have attempt to consider both consistency and specificity, they model the similarity matrix $\mathbf{A}^{(v)}$ with a consistent part \mathbf{S} and a specific part $\mathbf{S}^{(v)}$, i.e., $\mathbf{A}^{(v)} = \mathbf{S} + \mathbf{S}^{(v)}$. However, this model exists a significant limitation. It does not take into account the impact of noise, which leads to the noise being assigned to the specific component $\mathbf{S}^{(v)}$ during the learning process. As a consequence, the specific information learned is impure. Ideally, the specific component should reflect the unique information of each view that contributes

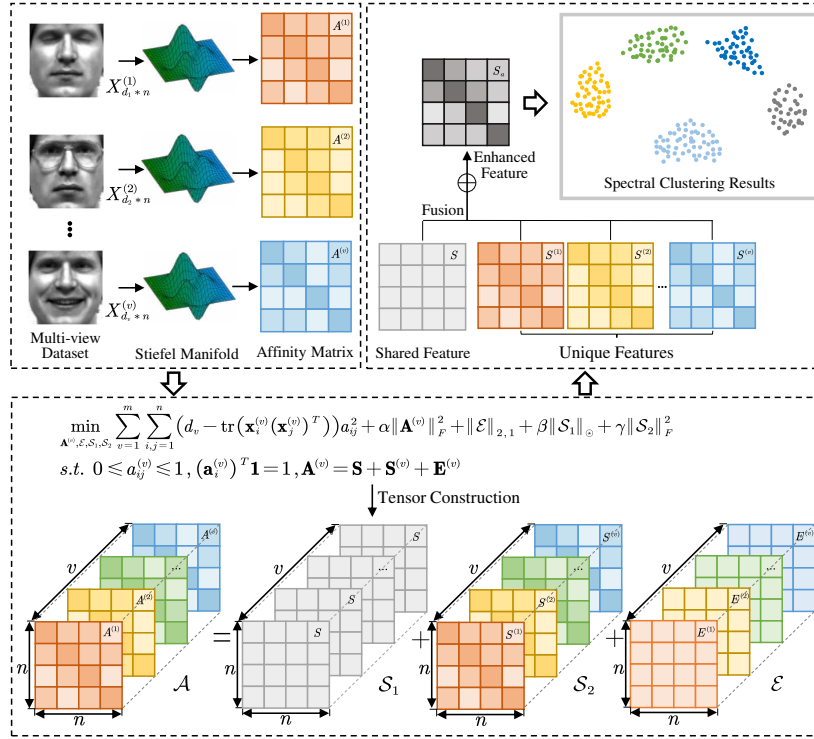


Fig. 1: Framework of CSTGL.

to achieve comprehensive information, rather than containing noise. Therefore, it is necessary to explicitly distinguish noise from specific information when modeling.

In order to tackle these limitations in the above observations, our goal is to design a novel graph learning framework that is equipped with an improved similarity measure for $\mathbf{A}^{(v)}$, as well as a noise-free graph fusion model that considers both consistency and specificity.

B. Model Formulation

For the purpose of capturing the intrinsic similarity between data points, we learn the neighbor graph for each view by measuring the similarity distance on the Stiefel manifold. Before proceeding, we briefly introduce the distance measure on the Stiefel manifold.

Stiefel manifold: The Stiefel manifold represents the set of matrices with orthonormal columns. The Stiefel manifold is commonly used in optimization and geometry, particular in problems involving rotations and orthogonal transformations. Given two $d \times n$ orthonormal matrices \mathbf{X} and \mathbf{Y} , the l_1 -norm geodesic distance between them is defined as [49]

$$d_s(\mathbf{X}, \mathbf{Y}) = d - \text{tr}(\mathbf{X}^T \mathbf{Y}). \quad (9)$$

Inspired from (9), a natural variant that involves two vectors \mathbf{x} and \mathbf{y} can be formulated to serve as a distance measure on the Stiefel manifold

$$d_s(\mathbf{x}, \mathbf{y}) = d - \text{tr}(\mathbf{x}\mathbf{y}^T), \quad (10)$$

where d can be interpreted as a threshold to guarantee the distance to be positive.

Remark 1: From (10), we have the subsequent observations. If $\text{tr}(\mathbf{x}\mathbf{y}^T) = 0$, then \mathbf{x} and \mathbf{y} are orthonormal to each other, implying that there is no similarity between them. If $\text{tr}(\mathbf{x}\mathbf{y}^T)$ is not zero, then \mathbf{x} and \mathbf{y} are not orthonormal to each other, and there exists some similarity between them. In summary, (10) can reflect the similarity between \mathbf{x} and \mathbf{y} . The greater the deviation between d and $\text{tr}(\mathbf{x}\mathbf{y}^T)$, the lower the similarity between \mathbf{x} and \mathbf{y} . Instead, smaller deviation implies higher similarity.

From the above discussion, we can define a new formulation to learn the neighbor graph $\mathbf{A}^{(v)}$, that is

$$\begin{aligned} \min_{\mathbf{A}^{(v)}} \sum_{v=1}^m \sum_{i,j=1}^n (d_v - \text{tr}(\mathbf{x}_i^{(v)} \mathbf{x}_j^{(v)T})) a_{ij}^2 + \alpha \|\mathbf{A}^{(v)}\|_F^2, \\ \text{s.t. } 0 \leq a_{ij}^{(v)} \leq 1, (\mathbf{a}_i^{(v)})^T \mathbf{1} = 1, \end{aligned} \quad (11)$$

where α denotes the positive balance parameter, and $\mathbf{a}_i^{(v)} \in \mathbb{R}^{n \times 1}$ is a column vector with its j -th element being $a_{ij}^{(v)}$. The main difference between the traditional neighbor graph learning and our method exists in the distance measure. In contrast to the traditional approach that utilizes Euclidean distance $\|\mathbf{x}_i^{(v)} - \mathbf{x}_j^{(v)}\|_2^2$ to measure similarity, our method uses Stiefel manifold distance, which more precisely reflects the intrinsic structure for real-world data.

After learning the neighbor graphs of all the views, we need to fuse these neighbor graphs. As mentioned in *Observations 2 and 3* of the motivation subsection, most graph-based multi-view methods follows (7) to learn a consensus graph, thereby ignoring the specific information of each view. While a few works consider both consistency and specificity, they fail to distinguish noise from specific information. To address

these limitations, we suppose that each neighbor graph $\mathbf{A}^{(v)}$ can be modelled by a consistent component, a view-specific component, and a noise component, i.e.,

$$\mathbf{A}^{(v)} = \mathbf{S} + \mathbf{S}^{(v)} + \mathbf{E}^{(v)}, \quad (12)$$

where \mathbf{S} denotes the consistent part, $\mathbf{S}^{(v)}$ represents the view-specific component, and $\mathbf{E}^{(v)}$ is the noise term.

Remark 2: In contrast to the model presented in *Observation 3*, our model explicitly separates the noise term from the specific component, which guarantees that the specific information learned is useful and free from noise. In essence, our modelling technique contributes to noise-free graph fusion.

For capturing the high-order correlation among different neighbor graphs, we formulate the following tensor-based graph fusion framework:

$$\begin{aligned} \min_{\mathbf{A}^{(v)}, \mathcal{E}, \mathcal{S}_1, \mathcal{S}_2} & \sum_{v=1}^m \sum_{i,j=1}^n (d_v - \text{tr}(\mathbf{x}_i^{(v)}(\mathbf{x}_j^{(v)})^T)) a_{ij}^2 + \alpha \|\mathbf{A}^{(v)}\|_F^2 \\ & + \|\mathcal{E}\|_{2,1} + \beta \|\mathcal{S}_1\|_{\otimes} + \gamma \|\mathcal{S}_2\|_F^2 \\ \text{s.t. } & 0 \leq a_{ij}^{(v)} \leq 1, (\mathbf{a}_i^{(v)})^T \mathbf{1} = 1, \mathbf{A}^{(v)} = \mathbf{S} + \mathbf{S}^{(v)} + \mathbf{E}^{(v)}, \end{aligned} \quad (13)$$

where $\mathcal{E} = \Phi(\mathbf{E}^{(1)}, \dots, \mathbf{E}^{(v)})$ is the noise tensor, $\mathcal{S}_1 = \Phi(\mathbf{S}, \dots, \mathbf{S})$ denotes the consistent tensor, $\mathcal{S}_2 = \Phi(\mathbf{S}^{(1)}, \dots, \mathbf{S}^{(v)})$ represents the specific tensor, they are all of size $n \times n \times m$, β and γ are trade-off parameters.

Remark 3: We impose $l_{2,1}$ -norm on the noise tensor \mathcal{E} to encourage the columns of each frontal slice \mathbf{E}^v to be zero, which is expected to minimize the impact of noise [9]. We enforce the consistent tensor \mathcal{S}_1 with the t -SVD based tensor nuclear norm to exploit more shared high-order information across various neighbor graphs [35]. Moreover, we impose F -norm on the specific tensor \mathcal{S}_2 in order to ensure the preservation of view-specific information.

C. Optimization

To handle the optimization problem in (13), we utilize the Alternating Direction Method of Multipliers (ADMM) [50] that is commonly used for solving multivariate constrained optimization problems. The core idea of ADMM is to solve each variable-induced subproblem by holding the other variables constant.

To proceed, we need to introduce two auxiliary variables to make our objective function separable. Let $\mathcal{E} = \mathcal{W}$ and $\mathcal{S}_1 = \mathcal{K}$, the original objective function can be equivalently described by

$$\begin{aligned} \min_{\mathbf{A}^{(v)}, \mathcal{W}, \mathcal{K}, \mathcal{S}_2, \mathcal{S}_1, \mathcal{E}} & \sum_{v=1}^m \sum_{i,j=1}^n (d_v - \text{tr}(\mathbf{x}_i^{(v)}(\mathbf{x}_j^{(v)})^T)) a_{ij}^2 \\ & + \alpha \|\mathbf{A}^{(v)}\|_F^2 + \|\mathcal{W}\|_{2,1} + \beta \|\mathcal{K}\|_{\otimes} + \gamma \|\mathcal{S}_2\|_F^2 \\ \text{s.t. } & 0 \leq a_{ij}^{(v)} \leq 1, (\mathbf{a}_i^{(v)})^T \mathbf{1} = 1, \mathbf{A}^{(v)} = \mathbf{S} + \mathbf{S}^{(v)} + \mathbf{E}^{(v)}, \\ & \mathcal{E} = \mathcal{W}, \mathcal{S}_1 = \mathcal{K}. \end{aligned} \quad (14)$$

As (12) can also be written as a tensor-shaped model, i.e., $\mathcal{A} = \mathcal{S}_1 + \mathcal{S}_2 + \mathcal{E}$, the corresponding augmented Lagrangian function of (14) is given by

$$\begin{aligned} \min_{\mathbf{A}^{(v)}, \mathcal{W}, \mathcal{K}, \mathcal{S}_2, \mathcal{S}_1, \mathcal{E}} & \sum_{v=1}^m \sum_{i,j=1}^n (d_v - \text{tr}(\mathbf{x}_i^{(v)}(\mathbf{x}_j^{(v)})^T)) a_{ij}^2 \\ & + \alpha \|\mathbf{A}^{(v)}\|_F^2 + \|\mathcal{W}\|_{2,1} + \beta \|\mathcal{K}\|_{\otimes} + \gamma \|\mathcal{S}_2\|_F^2 \\ & + \frac{\rho}{2} \|\mathcal{S}_1 + \mathcal{S}_2 + \mathcal{E} - (\mathcal{A} + \frac{\mathcal{Q}_1}{\rho})\|_F^2 \\ & + \frac{\rho}{2} \|\mathcal{K} - (\mathcal{S}_1 + \frac{\mathcal{Q}_2}{\rho})\|_F^2 \\ & + \frac{\rho}{2} \|\mathcal{W} - (\mathcal{E} + \frac{\mathcal{Q}_3}{\rho})\|_F^2 \\ \text{s.t. } & 0 \leq a_{ij}^{(v)} \leq 1, (\mathbf{a}_i^{(v)})^T \mathbf{1} = 1, \end{aligned} \quad (15)$$

where $\mathcal{Q}_1, \mathcal{Q}_2, \mathcal{Q}_3$ are the Lagrange multipliers with size $n \times n \times m$, and ρ is a positive factor. By applying the alternating minimization strategy, we decompose the optimization problem in (15) into the subsequent subproblems.

1) $\mathbf{A}^{(v)}$ -subproblem

We treat $\mathbf{A}^{(v)}$ as a variable while fixing other variables, resulting in

$$\begin{aligned} \min_{0 \leq a_{ij}^{(v)} \leq 1, (\mathbf{a}_i^{(v)})^T \mathbf{1} = 1} & \sum_{v=1}^m \sum_{i,j=1}^n (d_v - \text{tr}(\mathbf{x}_i^{(v)}(\mathbf{x}_j^{(v)})^T)) a_{ij}^2 \\ & + \alpha \|\mathbf{A}^{(v)}\|_F^2 + \frac{\rho}{2} \|\mathcal{S}_1 + \mathcal{S}_2 + \mathcal{E} - (\mathcal{A} + \frac{\mathcal{Q}_1}{\rho})\|_F^2 \end{aligned} \quad (16)$$

By denoting $\mathbf{B}^{(v)} = \mathbf{S} + \mathbf{S}^{(v)} + \mathbf{E}^{(v)} - \frac{\mathcal{Q}_1^{(v)}}{\rho}$ and $\mathbf{b}_i^{(v)}$ as a vector with its j -th entry being $b_{ij}^{(v)}$, the above equation can be written as

$$\begin{aligned} \min_{0 \leq a_{ij}^{(v)} \leq 1, (\mathbf{a}_i^{(v)})^T \mathbf{1} = 1} & \sum_{i,j=1}^n (d_v - \text{tr}(\mathbf{x}_i^{(v)}(\mathbf{x}_j^{(v)})^T)) a_{ij}^2 \\ & + \alpha (a_{ij}^{(v)})^2 + \frac{\rho}{2} (a_{ij}^{(v)} - b_{ij}^{(v)})^2. \end{aligned} \quad (17)$$

Let $e_{ij}^{(v)} = d_v - \text{tr}(\mathbf{x}_i^{(v)}(\mathbf{x}_j^{(v)})^T)$, we can further reformulate the problem in (17) separately for each i

$$\begin{aligned} \min_{0 \leq a_{ij}^{(v)} \leq 1, (\mathbf{a}_i^{(v)})^T \mathbf{1} = 1} & (\mathbf{e}_i^{(v)})^T \mathbf{a}_i^{(v)} + \alpha \|\mathbf{a}_i^{(v)}\|_2^2 \\ & + \frac{\rho}{2} (\|\mathbf{a}_i^{(v)}\|_2^2 - 2(\mathbf{a}_i^{(v)})^T \mathbf{b}_i^{(v)} + \|\mathbf{b}_i^{(v)}\|_2^2), \end{aligned} \quad (18)$$

where $\mathbf{e}_i^{(v)}$ is a vector with its j -th entry being $e_{ij}^{(v)}$.

It is easy to derive that the optimization problem in (18) can be transformed to solve

$$\min_{0 \leq a_{ij}^{(v)} \leq 1, (\mathbf{a}_i^{(v)})^T \mathbf{1} = 1} \left\| \mathbf{a}_i^{(v)} - \frac{\rho \mathbf{b}_i^{(v)} - \mathbf{e}_i^{(v)}}{2\alpha + \rho} \right\|_2^2 \quad (19)$$

Since the problem in (19) is an Euclidean projection problem on the simplex space, we rewrite it as

$$\begin{aligned} \mathcal{L}(\mathbf{a}_i^{(v)}, \eta, \psi) = & \frac{1}{2} \left\| \mathbf{a}_i^{(v)} - \frac{\rho \mathbf{b}_i^{(v)} - \mathbf{e}_i^{(v)}}{2\alpha + \rho} \right\|_2^2 \\ & - \eta((\mathbf{a}_i^{(v)})^T \mathbf{1} - 1) - \psi^T \mathbf{a}_i^{(v)}, \end{aligned} \quad (20)$$

where η is a positive constant, and ψ represents a Lagrangian coefficient vector. By applying the Karush-Kuhn-Tucker condition [51], the final solution to (20) is

$$\mathbf{a}_i^{(v)*} = \left(\frac{\rho \mathbf{b}_i^{(v)} - \mathbf{e}_i^{(v)}}{2\alpha + \rho} + \eta \mathbf{1} \right)_+, \quad (21)$$

where $(x)_+ = \max(x, 0)$. After obtaining all $\mathbf{a}_i^{(v)}$, we can reshape them into the matrix or tensor form.

2) \mathcal{W} -subproblem

By keeping \mathcal{W} as a variable and maintaining other variables fixed, we arrive at

$$\min_{\mathcal{W}} \|\mathcal{W}\|_{2,1} + \frac{\rho}{2} \|\mathcal{W} - (\mathcal{E} + \frac{\mathcal{Q}_3}{\rho})\|_F^2. \quad (22)$$

Given that the $l_{2,1}$ -norm of a tensor is defined as the sum of the l_2 -norms for each fiber along the third mode, thus we have $\|\mathbf{W}_{(3)}\|_{2,1} = \|\mathcal{W}\|_{2,1}$. Similarly, according the definition of the F -norm of a tensor, it is straightforward to see $\|\mathbf{W}_{(3)} - (\mathbf{E}_{(3)} + \frac{\mathbf{Q}_3^{(3)}}{\rho})\|_F^2 = \|\mathcal{W} - (\mathcal{E} + \frac{\mathcal{Q}_3}{\rho})\|_F^2$. Thus, the problem in (22) is transformed to

$$\min_{\mathbf{W}_{(3)}} \|\mathbf{W}_{(3)}\|_{2,1} + \frac{\rho}{2} \|\mathbf{W}_{(3)} - (\mathbf{E}_{(3)} + \frac{\mathbf{Q}_3^{(3)}}{\rho})\|_F^2. \quad (23)$$

Let $\mathbf{C} = \mathbf{E}_{(3)} + \frac{\mathbf{Q}_3^{(3)}}{\rho}$, and according to [9], the problem in (23) takes the following closed-form solution

$$\mathbf{W}_{(3):i}^* = \begin{cases} \frac{\|\mathbf{C}_{:,i}\|_2 - \frac{1}{\rho}}{\|\mathbf{C}_{:,i}\|_2}, & \text{if } \|\mathbf{C}_{:,i}\|_2 > \frac{1}{\rho} \\ 0, & \text{otherwise,} \end{cases} \quad (24)$$

where $\mathbf{C}_{:,i}$ denotes the i -th column of \mathbf{C} . After obtaining $\mathbf{W}_{(3):i}^*$ of all columns, we can reshape them into the tensor form.

3) \mathcal{K} -subproblem

By ignoring irrelevant variables, we update \mathcal{K} by solving

$$\min_{\mathcal{K}} \beta \|\mathcal{K}\|_{\otimes} + \frac{\rho}{2} \|\mathcal{K} - (\mathcal{S}_1 + \frac{\mathcal{Q}_2}{\rho})\|_F^2. \quad (25)$$

Let $\mathcal{F} = \mathcal{S}_1 + \frac{\mathcal{Q}_2}{\rho}$, the problem in (25) can be solved by applying the tensor tubal-shrinkage operator [52], which takes the following closed-form solution:

$$\mathcal{K}^* = \mathcal{D}_{\frac{m\beta}{\rho}}(\mathcal{F}) = \mathcal{U} * \mathcal{D}_{\frac{m\beta}{\rho}}(\mathcal{G}) * \mathcal{V}^T, \quad (26)$$

where $\mathcal{F} = \mathcal{U} * \mathcal{G} * \mathcal{V}^T$, $\mathcal{D}_{\frac{m\beta}{\rho}}(\mathcal{G}) = \mathcal{G} * \mathcal{P}$, and \mathcal{P} is a f-diagonal tensor with its diagonal element in the Fourier domain being $\hat{\mathcal{P}}(i, i, j) = \max(1 - \frac{m\beta/\rho}{\hat{\mathcal{G}}(i,i,j)}, 0)$.

4) \mathcal{S}_2 -subproblem

In order to update \mathcal{S}_2 , we neglect irrelevant variables, and arrive at

$$\min_{\mathcal{S}_2} \gamma \|\mathcal{S}_2\|_F^2 + \frac{\rho}{2} \|\mathcal{S}_1 + \mathcal{S}_2 + \mathcal{E} - (\mathcal{A} + \frac{\mathcal{Q}_1}{\rho})\|_F^2. \quad (27)$$

Motivated from [48], the problem in (27) can be transformed to solve an equivalent problem in the Fourier domain:

$$\min_{\hat{\mathcal{S}}_2} \gamma \|\hat{\mathcal{S}}_2\|_F^2 + \frac{\rho}{2} \|\hat{\mathcal{S}}_2 - (\hat{\mathcal{A}} + \frac{\hat{\mathcal{Q}}_1}{\rho} - \hat{\mathcal{S}}_1 - \hat{\mathcal{E}})\|_F^2. \quad (28)$$

To go further, the solution to (28) can be derived slice-by-slice along the frontal direction

$$\min_{\hat{\mathcal{S}}_2^{(v)}} \gamma \|\hat{\mathcal{S}}_2^{(v)}\|_F^2 + \frac{\rho}{2} \|\hat{\mathcal{S}}_2^{(v)} - (\hat{\mathcal{A}}^{(v)} + \frac{\hat{\mathcal{Q}}_1^{(v)}}{\rho} - \hat{\mathcal{S}}_1^{(v)} - \hat{\mathcal{E}}^{(v)})\|_F^2. \quad (29)$$

By differentiating (29) and setting the result to zero, we have

$$\hat{\mathcal{S}}_2^{(v)} = \frac{\rho(\hat{\mathcal{A}}^{(v)} + \frac{\hat{\mathcal{Q}}_1^{(v)}}{\rho} - \hat{\mathcal{S}}_1^{(v)} - \hat{\mathcal{E}}^{(v)})}{2\gamma + \rho}. \quad (30)$$

After getting $\hat{\mathcal{S}}_2^{(v)}$, we obtain $\mathcal{S}_2^{(v)}$ by performing inverse FFT. Then, the tensor \mathcal{S}_2^* to be updated can be recovered from $\mathcal{S}_2^{(v)}$.

5) \mathcal{S}_1 -subproblem

By eliminating other variables except for \mathcal{S}_1 -related variables, we formulate the following optimization problem

$$\min_{\mathcal{S}_1} \frac{\rho}{2} \|\mathcal{S}_1 + \mathcal{S}_2 + \mathcal{E} - (\mathcal{A} + \frac{\mathcal{Q}_1}{\rho})\|_F^2 + \frac{\rho}{2} \|\mathcal{K} - (\mathcal{S}_1 + \frac{\mathcal{Q}_2}{\rho})\|_F^2. \quad (31)$$

In analogy to the problem solving in (27), we transform the original problem into an equivalent problem in the Fourier domain. By solving this equivalent problem, we obtain

$$\hat{\mathcal{S}}_1^{(v)} = \frac{\hat{\mathcal{K}}^{(v)} - \frac{\hat{\mathcal{Q}}_2^{(v)}}{\rho} - [\hat{\mathcal{S}}_2^{(v)} + \hat{\mathcal{E}}^{(v)} - (\hat{\mathcal{A}}^{(v)} + \frac{\hat{\mathcal{Q}}_1^{(v)}}{\rho})]}{2}. \quad (32)$$

In a similar fashion, the tensor \mathcal{S}_1^* can be recovered from $\hat{\mathcal{S}}_1^{(v)}$.

6) \mathcal{E} -subproblem

To update \mathcal{E} , we discard irrelevant variables and formulate an optimization problem as follows:

$$\min_{\mathcal{E}} \frac{\rho}{2} \|\mathcal{S}_1 + \mathcal{S}_2 + \mathcal{E} - (\mathcal{A} + \frac{\mathcal{Q}_1}{\rho})\|_F^2 + \frac{\rho}{2} \|\mathcal{W} - (\mathcal{E} + \frac{\mathcal{Q}_3}{\rho})\|_F^2. \quad (33)$$

Following the similar procedures of solving subproblems \mathcal{S}_2 and \mathcal{S}_1 , the solution to (33) is given by

$$\hat{\mathcal{E}}^{(v)} = \frac{\hat{\mathcal{A}}^{(v)} + \frac{\hat{\mathcal{Q}}_1^{(v)}}{\rho} + \hat{\mathcal{W}}^{(v)} - \hat{\mathcal{S}}_1^{(v)} - \hat{\mathcal{S}}_2^{(v)} - \frac{\hat{\mathcal{Q}}_3^{(v)}}{\rho}}{2}. \quad (34)$$

From (34), we are able to construct the tensor \mathcal{E}^* that needs to be updated.

7) Updating multipliers

By performing the gradient ascent operation, we update the Lagrange multipliers as follows

$$\begin{cases} \mathcal{Q}_1 = \mathcal{Q}_1 + \rho(\mathcal{A} - (\mathcal{S}_1 + \mathcal{S}_2) - \mathcal{E}) \\ \mathcal{Q}_2 = \mathcal{Q}_2 + \rho(\mathcal{S}_1 - \mathcal{K}) \\ \mathcal{Q}_3 = \mathcal{Q}_3 + \rho(\mathcal{E} - \mathcal{W}) \end{cases} \quad (35)$$

where $\rho = \mu\rho$ with μ being a positive value.

Remark 4: After obtaining the learned consistent tensor \mathcal{S}_1 and view-specific tensor \mathcal{S}_2 , we require to fuse them to achieve the final graph matrix \mathbf{S}_a . A natural fusion scheme is to average the accumulation of all the frontal slices of \mathcal{S}_1 and \mathcal{S}_2 , which is defined by

$$\mathbf{S}_a = \frac{1}{m} \sum_{v=1}^m (\mathbf{S}_1^{(v)} + \mathbf{S}_2^{(v)}). \quad (36)$$

After obtaining the learned fusion graph \mathbf{S}_a , we construct the affinity matrix \mathbf{S}_{af} using $\mathbf{S}_{af} = \frac{\mathbf{S}_a + \mathbf{S}_a^T}{2}$, and then perform clustering. For the sake of clarity, we summarize the procedures of executing CSTGL in the Algorithm 1.

Algorithm 1 Procedures for optimization in CSTGL

Input: Multi-view data $\{\mathbf{X}^{(v)}\}_{v=1}^m$, parameters α, β and γ .
Initialize: Initialize $\mathbf{A}^{(v)}$ with probabilistic k -nearest neighbors; $\mathbf{W}^{(v)} = \mathbf{0}$, $\mathbf{K}^{(v)} = \mathbf{0}$, $\mathbf{S}_1^{(v)} = \mathbf{0}$, $\mathbf{S}_2^{(v)} = \mathbf{0}$, $\mathbf{E}^{(v)} = \mathbf{0}$, $\mathbf{Q}_1^{(v)} = \mathbf{0}$, $\mathbf{Q}_2^{(v)} = \mathbf{0}$, $\mathbf{Q}_3^{(v)} = \mathbf{0}$; $\mu = 2$, $\rho = 0.1$; $\mathbf{S}_a = \mathbf{0}$.

- 1: **while** not converged **do**
- 2: **for** $\forall v = 1, \dots, m$ **do**
- 3: Update $\mathbf{A}^{(v)}$ according to *subproblem 1*.
- 4: **end for**
- 5: Update $\mathcal{W}, \mathcal{K}, \mathcal{S}_2, \mathcal{S}_1, \mathcal{E}$ according to *subproblems 2-6*.
- 6: Update multipliers $\mathcal{Q}_1, \mathcal{Q}_2, \mathcal{Q}_3, \rho$ according to *subproblem 7*.
- 7: **end while**
- 8: Calculate the final graph matrix \mathbf{S}_a using Eq. (36).

Output: The learned fusion graph \mathbf{S}_a .

D. Computational Complexity

The main complexity of CSTGL contains the cost of solving 6 subproblems. As the update of Lagrange multipliers involves matrix addition operations, we ignore its complexity. The detailed computational complexity analysis is presented below. For the $\mathbf{A}^{(v)}$ -subproblem, the complexity of calculating (21) for a single view takes $O(n^2)$, resulting in a total computational complexity of $O(mn^2)$ for all views. For the \mathcal{W} -subproblem, it consumes a complexity of $O(mn^2)$. For the \mathcal{K} -subproblem, the complexity includes performing the FFT and inverse FFT of a $n \times n \times m$ tensor, as well as executing the SVD in the Fourier domain, which requires $O(mn^3 + mn^2 \log(m))$ [36]. The updates of $\mathcal{S}_2, \mathcal{S}_1$ and \mathcal{E} have similar solving procedures, all involving FFT and inverse FFT operations, which takes $O(mn^2 \log(m))$. Therefore, the entire complexity of solving CSTGL is $O(mn^3 + mn^2 \log(m) + mn^2)$.

IV. SIMULATIONS

In this section, we conduct comprehensive experiments to validate the effectiveness of CSTGL. To be specific, we carry out the clustering performance and affinity matrix visualization comparison. We also conduct the parameter sensitivity and convergence analysis, and compare the running time of various methods. All experiments are conducted on a computer equipped with a 12th Generation Intel(R) Core(TM) i5-12490F CPU. Experimental results are obtained by averaging 10 trials.

A. Experimental Settings

1) *Datasets:* We select six representative real-world multi-view datasets, a brief description on them is given below:

HW¹: It is composed of 2,000 data points for digits 0 and 9 from UCI machine learning repository and two public features are available.

Reuters²: It contains 18,785 documents written in five different languages: French, Italian, English, German, and

Spanish. We use 600 documents from 6 categories in our experiments.

BBCSport³: This dataset contains 544 documents sourced from the BBC Sport website, covering news from five different categories. In the experiments, two views with dimensions of 3,183 and 3,203 are selected.

3-sources⁴: This dataset includes 948 news articles covering 416 unique news stories. These articles are collected from three well-known online news sources. For our experiments, we use 169 articles that are classified into 6 categories across all three sources.

Yale⁵: It consists of 165 gray-scale images of 15 individuals with different facial expressions and configurations. Followed by [39], 4096 dimensions intensity feature, 3,304 LBP feature and 6,750 dimensions Gabor feature are extracted as three multi-view features.

WebKB⁶: This dataset consists of 203 web-pages of 4 classes. Each web-page is described by the content of the page, the anchor text of the hyper-link, and the text in its title.

2) *Compared Methods:* Several multi-view baselines are involved to perform comparison, they are:

MCGC [53]: This method proposes an effective disagreement cost function to learn the consensus graph.

CSMSC [18]: This method takes into account both consistent and specific information to perform subspace clustering.

LMSC [16]: This method aims to learn a latent representation for comprehensive information recovery.

MCLES [54]: This method clusters multi-view data in a learned latent embedding space.

t-SVD-MS [35]: This method applies the t-SVD based tensor nuclear norm to capture high-order information among views.

WTSNM [55]: This method investigates the weighted tensor Schatten p -norm in the tensor-singular value decomposition.

TBGL [41]: This method designs a variance-based de-correlation anchor selection strategy for bipartite graph.

LTBPL [39]: This method integrates the low-rank probability matrices and the consensus indicator graph into a framework.

UDBG [56]: This method unifies the learning of the view-specific and consensus bipartite graph.

MMGC [57]: This method integrates the metric learning and graph learning to simplify the relationship among data.

SLMVGC [58]: This method attempts to explore the topological structure of data for performance improvement.

3) *Evaluation Metrics and Parameter Setting:* All the methods are evaluated by : clustering accuracy (ACC), normalized mutual information (NMI), adjusted rand index (ARI), and F1 score (Fscore). For a fair comparison, we carefully tune the parameters from the grid set $\{10^{-3}, 10^{-2}, 10^{-1}, 10^0, 10^1, 10^2, 10^3\}$ to achieve the optimal performance for all methods. Alternatively, we utilize recommended parameters if they are available for previous methods.

³<http://mlg.ucd.ie/datasets/bbc.html>

⁴<http://mlg.ucd.ie/datasets/3sources.html>

⁵<http://vision.ucsd.edu/content/yale-face-database>

⁶<http://www.webkb.org/webkb.html>

¹<https://cs.nyu.edu/~roweis/data.html>

²<https://lig-membres.imag.fr/grimal/data.html>

TABLE II: Evaluation metrics of all compared methods on HW, Reuters and BBCSport (%). Bold font indicates the highest performance, and underline font indicates the second-best performance.

Datasets	HW				Reuters				BBCSport			
	ACC	NMI	ARI	Fscore	ACC	NMI	ARI	Fscore	ACC	NMI	ARI	Fscore
MCGC	0.6890	0.6684	0.5653	0.6116	0.3167	0.2510	0.0431	0.2894	0.9743	0.9145	0.9376	0.9525
CSMSC	0.8959	0.8252	0.7944	0.8115	0.5043	0.3271	0.2288	0.3660	0.9559	0.8619	0.8882	0.9148
LMSC	0.8326	0.8152	0.7344	0.7605	0.3789	0.2711	0.1345	0.3246	0.8957	0.7953	0.7722	0.8325
MCLES	0.8277	0.8898	0.8054	0.8256	0.3721	0.3344	0.1298	0.3476	0.8908	0.8351	0.8475	0.8933
t-SVD-MSC	0.9885	0.9859	0.9867	0.9870	0.3633	0.2101	0.1186	0.3045	0.9706	0.9049	0.9172	0.9371
WTSNM	0.6565	0.5804	0.5040	0.5539	0.3717	0.1515	0.1099	0.2576	0.5074	0.2348	0.1672	0.3486
TBGL	0.9805	0.9604	0.9554	0.9598	0.2133	0.1265	0.0068	0.2822	0.5202	0.2508	0.1340	0.4276
LTBPL	<u>0.9990</u>	<u>0.9973</u>	<u>0.9978</u>	<u>0.9980</u>	<u>0.9600</u>	<u>0.9180</u>	<u>0.9086</u>	<u>0.9238</u>	0.9982	0.9924	0.9941	0.9955
UDBGL	0.6770	0.5900	0.4791	0.5449	0.3583	0.1412	0.1154	0.2908	0.4963	0.1940	0.2425	0.4865
MMGC	0.5610	0.5321	0.3999	0.4621	0.6367	0.4445	0.3860	0.4931	0.9596	0.8753	0.8931	0.9183
SLMVG	0.7205	0.6880	0.5938	0.6363	0.3693	0.1348	0.0743	0.2554	0.7478	0.5763	0.4871	0.6060
Ours	1.0000	1.0000	1.0000	1.0000	0.9983	0.9948	0.9960	0.9966	<u>0.9963</u>	<u>0.9854</u>	<u>0.9907</u>	<u>0.9929</u>

TABLE III: Evaluation metrics of all compared methods on 3-sources, Yale and WebKB (%). Bold font indicates the highest performance, and underline font indicates the second-best performance.

Datasets	3-sources				Yale				WebKB			
	ACC	NMI	ARI	Fscore	ACC	NMI	ARI	Fscore	ACC	NMI	ARI	Fscore
MCGC	0.4793	0.2737	0.0879	0.3911	0.6242	0.6517	0.4409	0.4767	0.7241	0.3016	0.3767	0.6489
CSMSC	0.6509	0.4836	0.4658	0.5840	0.7044	0.7135	0.5421	0.5637	0.6502	0.2985	0.3313	0.6085
LMSC	0.5266	0.3897	0.3097	0.4603	0.7421	0.7538	0.5844	0.6101	0.7340	0.3107	0.3926	0.6592
MCLES	0.6864	0.5904	0.4461	0.6100	0.6976	0.7290	0.5005	0.5341	0.6976	0.7290	<u>0.5005</u>	0.5341
t-SVD-MSC	0.6391	0.6043	0.4958	0.6007	<u>0.7455</u>	0.8011	0.6237	0.6481	0.7143	0.4132	<u>0.4503</u>	0.6650
WTSNM	0.4024	0.3522	0.1590	0.3407	0.7333	0.7186	0.5101	0.5416	0.6108	0.2546	0.2731	0.5509
TBGL	0.3491	0.1011	0.0143	0.3683	0.6909	0.7253	0.5006	0.5347	0.6305	0.2734	0.1919	0.5401
LTBPL	0.6686	0.4372	0.4134	0.5985	<u>0.7455</u>	0.7868	<u>0.6358</u>	<u>0.6589</u>	0.5714	0.0666	0.0556	0.5755
UDBGL	0.4142	0.1720	0.1031	0.3410	0.5515	0.6227	0.3761	0.4192	<u>0.7685</u>	0.3902	0.4817	<u>0.7072</u>
MMGC	<u>0.7219</u>	<u>0.5758</u>	<u>0.5221</u>	<u>0.6178</u>	<u>0.7455</u>	0.7557	0.5675	0.5957	0.6650	0.4070	0.4269	0.6084
SLMVG	0.6219	0.4540	0.3650	0.5214	0.6224	0.6292	0.4042	0.4417	0.7094	0.2767	0.3194	0.6363
Ours	0.7757	0.6797	0.6264	0.7202	0.7697	<u>0.7956</u>	0.6381	0.6608	0.7733	<u>0.4213</u>	0.5309	0.7335

B. Experimental Results

1) *Clustering Comparison*: We record the evaluation metrics of different methods on six datasets in Tables II and III. In particular, Table II reports the clustering results on the HW, Reuters and BBCsport datasets, while Table III shows the clustering performance on the 3-sources, Yale and WebKB datasets. From the table results, we have some findings below:

a) Our proposed CSTGL exhibits the best clustering performance on most tested datasets. Specifically, it achieves the top performance in terms of all the evaluation metrics on the HW, Reuters and 3-sources datasets. Simultaneously, it shows the best performance in terms of ACC, ARI and Fscore on the Yale and WebKB datasets. For example, CSTGL achieves a perfect score of 100% in ACC, NMI, ARI and Fscore on the HW dataset. On the 3-sources dataset, CSTGL shows an accuracy of 77.57%, marking an improvement of 5.38% compared to the second-performing method, MMGC. On Yale and WebKB, CSTGL continues to achieve the highest accuracy, reaching 76.97% and 77.33% respectively. Despite that CSTGL ranks the second-best method on the BBCsport, all of its evaluation metrics are quite close to those of the top-performing method, LTBPL.

b) Multi-view methods with both consistent and view-specific information considered generally outperform those methods that only consider consistency among views. For example, CSMSC, a representative subspace clustering method

that exploits both consistency and specificity, behaves better than MCGC on the HW, Reuters, 3-sources, and Yale datasets. It achieves an accuracy improvement of 20.69%, 18.76%, 17.16%, and 8.02%, respectively. In addition, methods based on latent representation, such as LMSC and MCLES, while not offering the best, still provide commendable performance. This originates from the fact that latent representation-based methods explore comprehensive information from the potential latent space.

c) Generally, tensor-based multi-view methods outperform other non-tensor-based competing methods. For example, previous methods such as t-SVD-MSC and LTBPL demonstrate clustering performance that is only second to our proposed method on the HW dataset, achieving accuracies of 98.85% and 99.9%, respectively. This superior performance can be attributed to the comprehensive consideration of high-order information by tensor decomposition. In contrast to these previous tensor-based methods, our proposed method, CSTGL, exhibits even better clustering performance. This can be largely attributed to its capability to capture the underlying structure of data on the Stiefel manifold, and the utilization of a newly designed tensor-based graph learning model that ensures both consistency and specificity, while effectively excluding the influence of noise.

2) *Ablation Studies*: To validate the advantages of similarity measure on Stiefel manifold and tensor graph fusion,

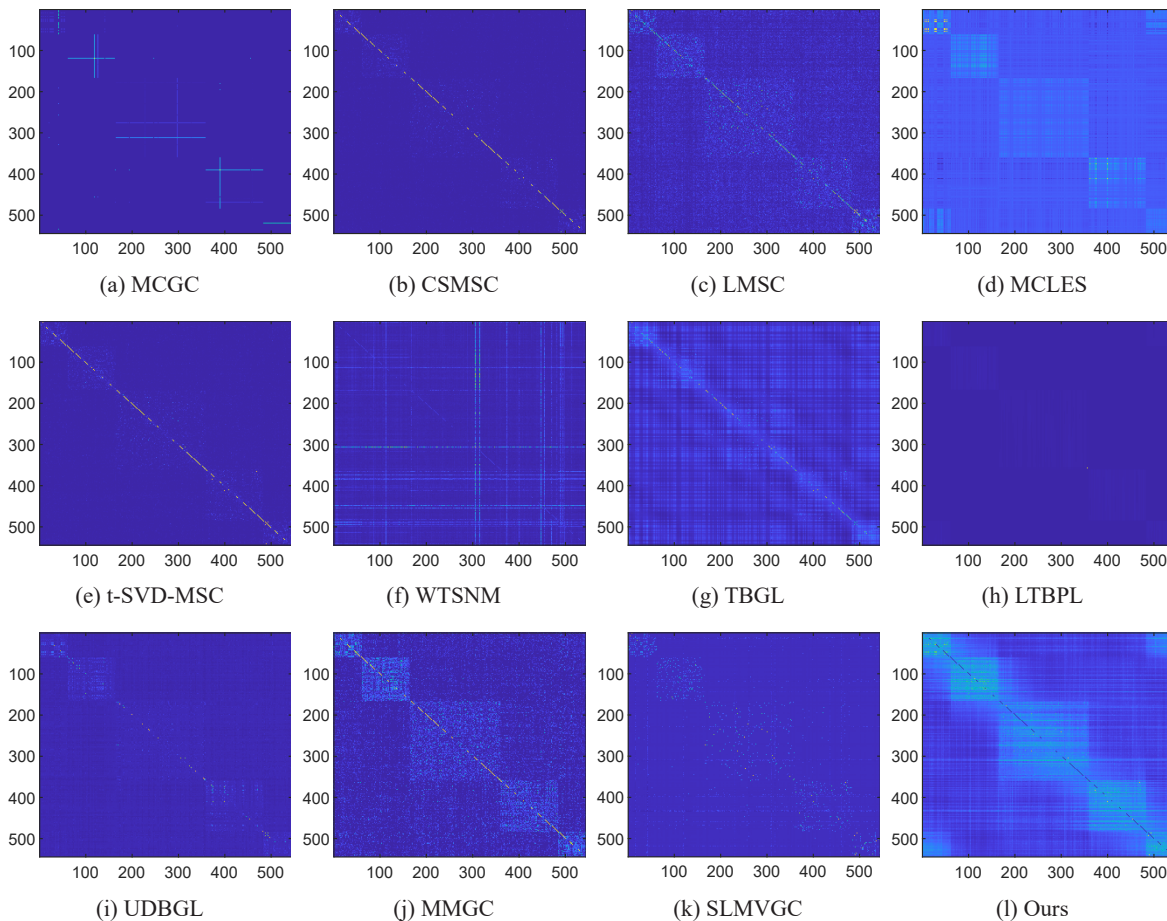


Fig. 2: Visualization of affinity matrix on BBCSport.

TABLE IV: Ablation studies of CSTGL using different distance measures on various datasets, and the metric ACC is employed. (a) Euclidean distance, and (b) Stiefel manifold distance.

dis	HW	Reuters	BBCsport	3-sources	Yale	Webkb
(a)	1.0000	0.9933	0.9467	0.7870	0.7479	0.7291
(b)	1.0000	0.9983	0.9963	0.7757	0.7697	0.7783

we conduct corresponding ablation studies. Specifically, when investigating the effects of using different distance measures, we alternate the similarity measure between Euclidean distance and Stiefel manifold distance while maintaining all other implementation procedures unchanged. When exploring the benefits of tensor graph fusion, we examine the effects of discarding the consistent tensor \mathcal{S}_1 and specific tensor \mathcal{S}_2 , individually.

Table IV records the experimental results of CSTGL using different distance measures on various datasets. It is seen that for most tested datasets, the performance of CSTGL using Euclidean distance is inferior to that using Stiefel manifold distance. However, for the 3-sources dataset, CSTGL exhibits weaker performance when using the Stiefel manifold. This can be attributed to the nature of the 3-sources dataset, which is news-related, and the data may be sparse due to the limitation of news sources. In such a scenario, Euclidean distance, without considering the intrinsic structure of the data, could

be more effective.

Table V shows the ablation studies of tensor graph fusion on the BBCSport, 3-sources, and WebKB datasets. From an overall perspective, both the consistent tensor graph and specific tensor graph contribute to the performance improvement of CSTGL. In particular, on the BBCSport and WebKB datasets, the consistent component contributes more significantly than the specific component, while on the 3-sources dataset, the specific component has a slightly greater contribution than the consistent component.

3) *Visualization of Affinity Matrix*: In Fig. 2, we exhibit the visualization results of affinity matrices for all the compared multi-view methods on BBCSport. In the graph-based methods, these affinity matrices are commonly known similarity graphs. It is seen that by comparing the block-diagonal structures of various multi-view methods, our method exhibits a more distinct block-diagonal structure, despite having some shadows in the off-diagonal blocks. This further demonstrates that CSTGL can achieve satisfactory clustering performance.

4) *Parameter Sensitivity Analysis*: To measure the influence of parameter choices on the CSTGL’s performance, the parameter sensitivity analyses involving all the evaluation metrics on the BBCSport, HW, Yale and WebKB datasets are conducted, as shown in Fig. 3. By extensive experiments, we find that CSTGL is not sensitive to the selection of parameter α . Consequently, we fix $\alpha = 10$, and investigate

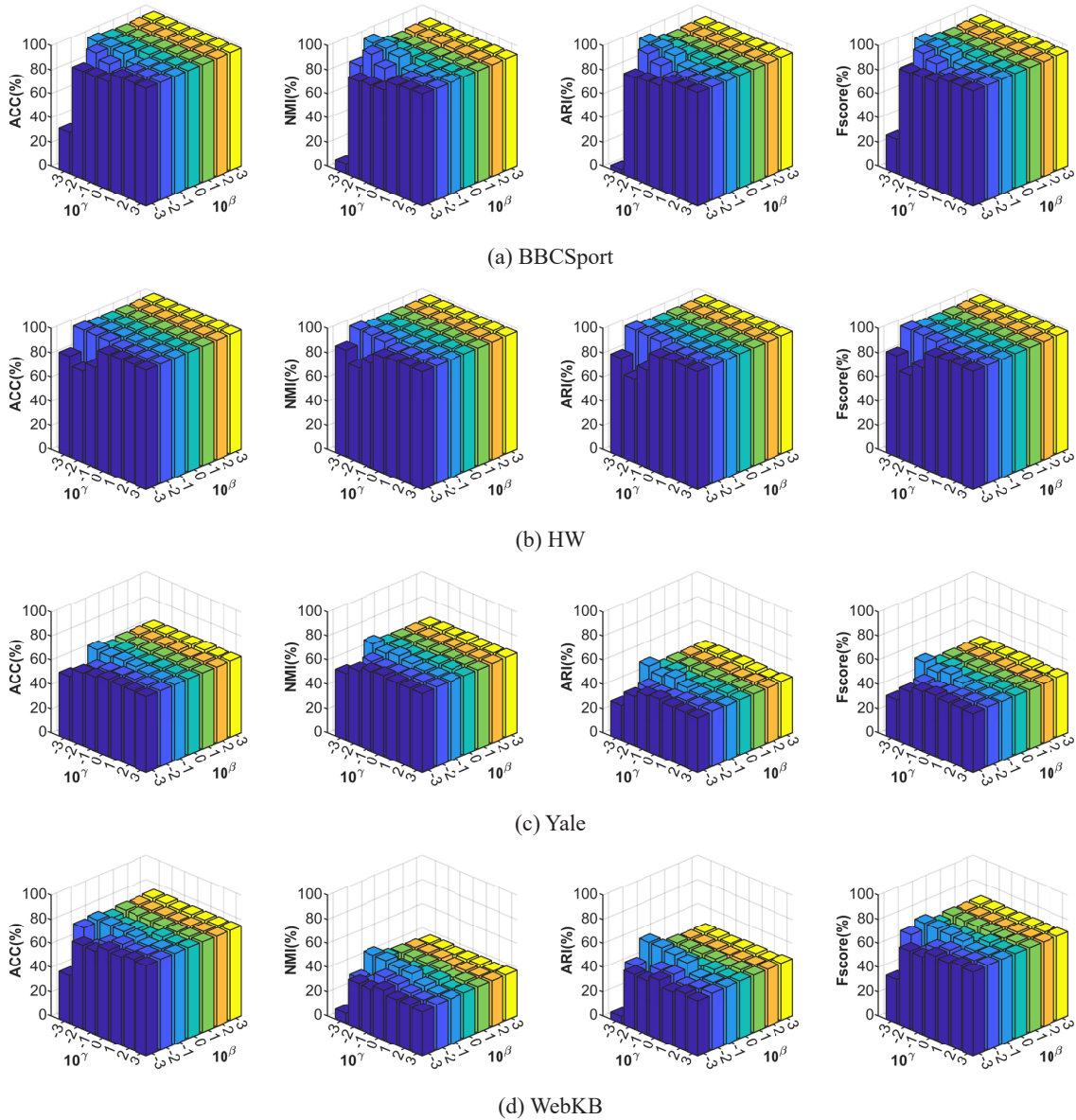


Fig. 3: Parameter sensitivity results on four datasets.

TABLE V: Ablation studies of tensor graph fusion on the BBCSport, 3-sources and WebKB datasets. (a) retaining consistent tensor graph, (b) retaining view-specific tensor graph, and (c) retaining both consistent and view-specific tensor graphs.

Cases	Components		BBCSport				3-sources				WebKB			
	Con.	Spe.	ACC	NMI	ARI	Fscore	ACC	NMI	ARI	Fscore	ACC	NMI	ARI	Fscore
(a)	✓		0.7188	0.8709	0.7425	0.7987	0.6094	0.6401	0.4367	0.5491	0.7290	0.4879	0.5293	0.7277
(b)		✓	0.3217	0.0844	0.0474	0.2545	0.6745	0.6267	0.4673	0.5725	0.0321	0.0460	0.0053	0.3141
(c)	✓	✓	0.9963	0.9854	0.9907	0.9929	0.7751	0.6783	0.6252	0.7193	0.7733	0.4213	0.5309	0.7335

the sensitivity induced by β and γ . Overall, it is observed that the performance of CSTGL does not significantly vary with the choice of β . However, it does exhibit sensitivity to the choice of γ , particularly when β is set to a small value. More specifically, when $\beta = 10^{-3}$, a decrease in γ leads to a deterioration in CSTGL’s performance. By referring to the objective function in (14), we can see that the parameter γ is used to regulate the view-specific tensor term. Therefore, we recommend using large γ to emphasize the view’s specificity

for desirable clustering performance.

5) *Empirical Convergence Analysis*: In multi-view clustering, ensuring consistency is an essential prerequisite. Therefore, focusing on the update related to consistency is a straightforward approach when investigating convergence. As a result, we plot the evolutionary curves of $\|\mathcal{S}_1^{k+1} - \mathcal{S}_1^k\|_F^2$ on six datasets. From Fig. 4, we see that the update of the consistent tensor \mathcal{S}_1 is convergent, arriving at the steady-state within 20 iterations. Although \mathcal{S}_1 experiences an ascent within

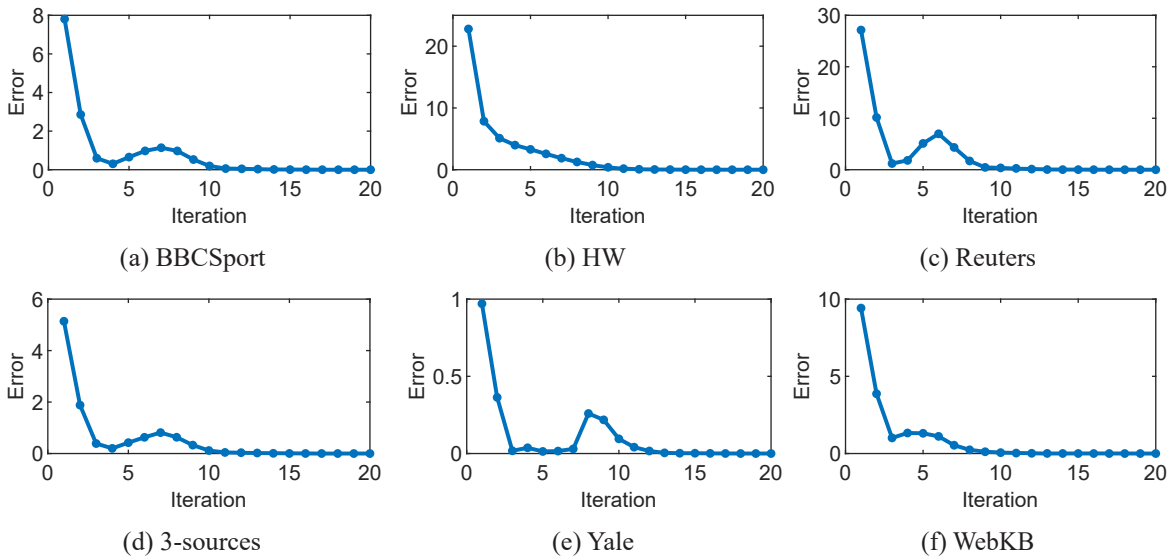


Fig. 4: Convergent behavior of CSTGL.

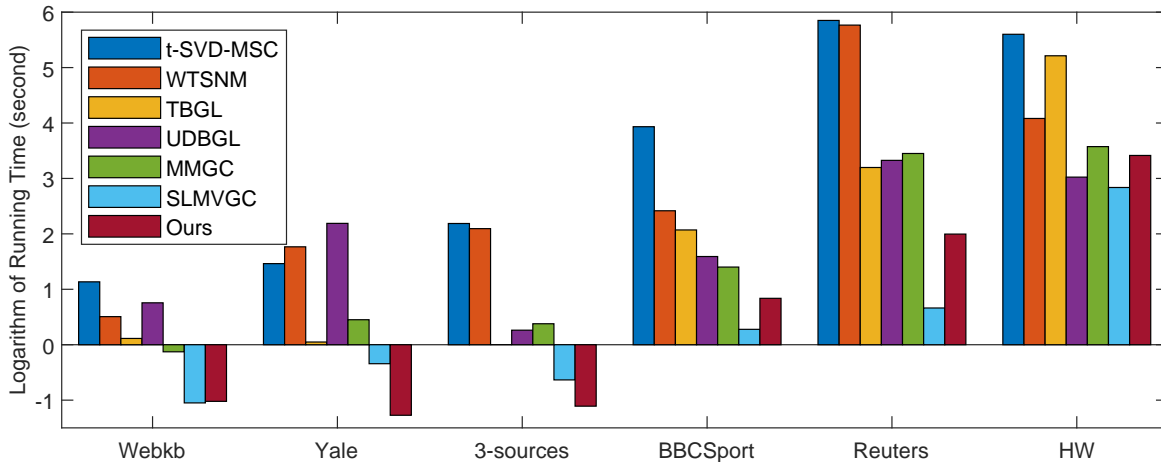


Fig. 5: Comparison of running time of various multi-view methods.

the iteration range of $[5, 10]$ on some datasets, it generally converges to the steady-state after 10 iterations. Slight oscillations during the convergence process of optimization are expected, especially when using gradient descent in the presence of noisy data.

6) *Running Time*: To intuitively show the computational cost of CSTGL, we plot a bar chart to compare the actual running times of various multi-view methods, as shown in Fig. 5. The Y-axis of the bar chart represents the logarithmic running time. Our method nearly achieves the fastest running time on the WebKB, Yale, and 3-sources datasets. The logarithmic running time is around -1 , which corresponds to an actual running time of approximate 0.35 seconds. On the BBCSport, Reuters and HW datasets, our method continues to demonstrate a competitive advantage in terms of running time. More specifically, our CSTGL outperforms previous t-SVD-MSc and WTSNM which are two typical tensor-based methods.

V. CONCLUSION

We propose a novel tensor-based graph learning framework, namely CSTGL. Our work makes two significant contributions in 1) the learning of neighbor graph, and 2) the model of graph fusion. Firstly, we learn the neighbor graph of each view based on using the Stiefel manifold distance, which is empirically verified to more effectively recover the intrinsic structure than using Euclidean distance. Secondly, after obtaining the learned neighbor graphs for all views, we formulate a tensor-based graph fusion model by assuming that the neighbor graph of each view is composed of a consistent graph, a view-specific graph, and a noise term. This model considers both consistency and specificity, while avoiding the issue of potential noise contamination in the learned specific information. Additionally, thanks to the t-SVD based tensor nuclear norm, CSTGL is capable of capturing high-order correlations among different views. Extensive experiments have demonstrated that CSTGL outperforms some SOTA multi-view methods.

REFERENCES

- [1] R. Zhang, F. Nie, X. Li, and X. Wei, "Feature selection with multi-view data: A survey," *Information Fusion*, vol. 50, pp. 158–167, 2019.
- [2] S. Yang, L. Li, S. Wang, W. Zhang, Q. Huang, and Q. Tian, "Skeletonnet: A hybrid network with a skeleton-embedding process for multi-view image representation learning," *IEEE Transactions on Multimedia*, vol. 21, no. 11, pp. 2916–2929, 2019.
- [3] Y. Fu, Y. Guo, Y. Zhu, F. Liu, C. Song, and Z.-H. Zhou, "Multi-view video summarization," *IEEE Transactions on Multimedia*, vol. 12, no. 7, pp. 717–729, 2010.
- [4] J. Zhao, X. Xie, X. Xu, and S. Sun, "Multi-view learning overview: Recent progress and new challenges," *Information Fusion*, vol. 38, pp. 43–54, 2017.
- [5] Y. Li, M. Yang, and Z. Zhang, "A survey of multi-view representation learning," *IEEE transactions on knowledge and data engineering*, vol. 31, no. 10, pp. 1863–1883, 2018.
- [6] Y. Chen, X. Xiao, C. Peng, G. Lu, and Y. Zhou, "Low-rank tensor graph learning for multi-view subspace clustering," *IEEE Transactions on Circuits and Systems for Video Technology*, vol. 32, no. 1, pp. 92–104, 2021.
- [7] Q. Shen, T. Xu, Y. Liang, Y. Chen, and Z. He, "Robust tensor recovery for incomplete multi-view clustering," *IEEE Transactions on Multimedia*, 2023.
- [8] H. Gao, F. Nie, X. Li, and H. Huang, "Multi-view subspace clustering," in *Proceedings of the IEEE international conference on computer vision*, 2015, pp. 4238–4246.
- [9] G. Liu, Z. Lin, S. Yan, J. Sun, Y. Yu, and Y. Ma, "Robust recovery of subspace structures by low-rank representation," *IEEE transactions on pattern analysis and machine intelligence*, vol. 35, no. 1, pp. 171–184, 2012.
- [10] E. Elhamifar and R. Vidal, "Sparse subspace clustering: Algorithm, theory, and applications," *IEEE Transactions on Pattern Analysis and Machine Intelligence*, vol. 35, no. 11, pp. 2765–2781, 2013.
- [11] X. Peng, Z. Yu, Z. Yi, and H. Tang, "Constructing the l2-graph for robust subspace learning and subspace clustering," *IEEE transactions on cybernetics*, vol. 47, no. 4, pp. 1053–1066, 2016.
- [12] L. Cao, L. Shi, J. Wang, Z. Yang, and B. Chen, "Robust subspace clustering by logarithmic hyperbolic cosine function," *IEEE Signal Processing Letters*, 2023.
- [13] M. Brbić and I. Kopriva, "Multi-view low-rank sparse subspace clustering," *Pattern Recognition*, vol. 73, pp. 247–258, 2018.
- [14] —, "l₀-motivated low-rank sparse subspace clustering," *IEEE Transactions on Cybernetics*, vol. 50, no. 4, pp. 1711–1725, 2018.
- [15] C. Zhang, Q. Hu, H. Fu, P. Zhu, and X. Cao, "Latent multi-view subspace clustering," in *Proceedings of the IEEE conference on computer vision and pattern recognition*, 2017, pp. 4279–4287.
- [16] C. Zhang, H. Fu, Q. Hu, X. Cao, Y. Xie, D. Tao, and D. Xu, "Generalized latent multi-view subspace clustering," *IEEE transactions on pattern analysis and machine intelligence*, vol. 42, no. 1, pp. 86–99, 2018.
- [17] D. Xie, X. Zhang, Q. Gao, J. Han, S. Xiao, and X. Gao, "Multiview clustering by joint latent representation and similarity learning," *IEEE transactions on cybernetics*, vol. 50, no. 11, pp. 4848–4854, 2019.
- [18] S. Luo, C. Zhang, W. Zhang, and X. Cao, "Consistent and specific multi-view subspace clustering," in *Proceedings of the AAAI conference on artificial intelligence*, vol. 32, no. 1, 2018.
- [19] W. Zhu, J. Lu, and J. Zhou, "Structured general and specific multi-view subspace clustering," *Pattern Recognition*, vol. 93, pp. 392–403, 2019.
- [20] L. Xing, B. Chen, S. Du, Y. Gu, and N. Zheng, "Correntropy-based multiview subspace clustering," *IEEE Transactions on Cybernetics*, vol. 51, no. 6, pp. 3298–3311, 2019.
- [21] M. Sun, P. Zhang, S. Wang, S. Zhou, W. Tu, X. Liu, E. Zhu, and C. Wang, "Scalable multi-view subspace clustering with unified anchors," in *Proceedings of the 29th ACM International Conference on Multimedia*, 2021, pp. 3528–3536.
- [22] Q. Gao, W. Xia, Z. Wan, D. Xie, and P. Zhang, "Tensor-svd based graph learning for multi-view subspace clustering," in *Proceedings of the AAAI Conference on Artificial Intelligence*, vol. 34, no. 04, 2020, pp. 3930–3937.
- [23] Z. Long, C. Zhu, J. Chen, Z. Li, Y. Ren, and Y. Liu, "Multi-view mera subspace clustering," *IEEE Transactions on Multimedia*, 2023.
- [24] Y. Liu, Y. Tan, H. Wu, S. Huang, Y. Ren, and J. Lv, "Preserving local and global information: An effective metric-based subspace clustering," in *Proceedings of the 31st ACM International Conference on Multimedia*, 2023, pp. 3619–3627.
- [25] F. Nie, J. Li, X. Li *et al.*, "Parameter-free auto-weighted multiple graph learning: a framework for multiview clustering and semi-supervised classification," in *IJCAI*, vol. 9, 2016.
- [26] —, "Self-weighted multiview clustering with multiple graphs," in *IJCAI*, 2017, pp. 2564–2570.
- [27] H. Wang, Y. Yang, and B. Liu, "Gmc: Graph-based multi-view clustering," *IEEE Transactions on Knowledge and Data Engineering*, vol. 32, no. 6, pp. 1116–1129, 2019.
- [28] R. Wang, F. Nie, Z. Wang, H. Hu, and X. Li, "Parameter-free weighted multi-view projected clustering with structured graph learning," *IEEE Transactions on Knowledge and Data Engineering*, vol. 32, no. 10, pp. 2014–2025, 2019.
- [29] Y. Liang, D. Huang, and C.-D. Wang, "Consistency meets inconsistency: A unified graph learning framework for multi-view clustering," in *2019 IEEE International Conference on Data Mining (ICDM)*. IEEE, 2019, pp. 1204–1209.
- [30] Z. Kang, C. Peng, Q. Cheng, X. Liu, X. Peng, Z. Xu, and L. Tian, "Structured graph learning for clustering and semi-supervised classification," *Pattern Recognition*, vol. 110, p. 107627, 2021.
- [31] Z. Li, C. Tang, X. Liu, X. Zheng, W. Zhang, and E. Zhu, "Consensus graph learning for multi-view clustering," *IEEE Transactions on Multimedia*, vol. 24, pp. 2461–2472, 2021.
- [32] J. Wen, K. Yan, Z. Zhang, Y. Xu, J. Wang, L. Fei, and B. Zhang, "Adaptive graph completion based incomplete multi-view clustering," *IEEE Transactions on Multimedia*, vol. 23, pp. 2493–2504, 2020.
- [33] H. Wang, G. Jiang, J. Peng, R. Deng, and X. Fu, "Towards adaptive consensus graph: multi-view clustering via graph collaboration," *IEEE Transactions on Multimedia*, 2022.
- [34] L. Xing, Y. Song, B. Chen, C. Yu, and J. Qin, "Incomplete multi-view clustering via correntropy and complement consensus learning," *IEEE Transactions on Multimedia*, 2024.
- [35] Y. Xie, D. Tao, W. Zhang, Y. Liu, L. Zhang, and Y. Qu, "On unifying multi-view self-representations for clustering by tensor multi-rank minimization," *International Journal of Computer Vision*, vol. 126, pp. 1157–1179, 2018.
- [36] J. Wu, Z. Lin, and H. Zha, "Essential tensor learning for multi-view spectral clustering," *IEEE Transactions on Image Processing*, vol. 28, no. 12, pp. 5910–5922, 2019.
- [37] Y. Tang, Y. Xie, C. Zhang, and W. Zhang, "Constrained tensor representation learning for multi-view semi-supervised subspace clustering," *IEEE Transactions on Multimedia*, vol. 24, pp. 3920–3933, 2021.
- [38] J. Wu, X. Xie, L. Nie, Z. Lin, and H. Zha, "Unified graph and low-rank tensor learning for multi-view clustering," in *Proceedings of the AAAI conference on artificial intelligence*, vol. 34, no. 04, 2020, pp. 6388–6395.
- [39] M.-S. Chen, C.-D. Wang, and J.-H. Lai, "Low-rank tensor based proximity learning for multi-view clustering," *IEEE Transactions on Knowledge and Data Engineering*, vol. 35, no. 5, pp. 5076–5090, 2022.
- [40] G. Jiang, J. Peng, H. Wang, Z. Mi, and X. Fu, "Tensorial multi-view clustering via low-rank constrained high-order graph learning," *IEEE Transactions on Circuits and Systems for Video Technology*, vol. 32, no. 8, pp. 5307–5318, 2022.
- [41] W. Xia, Q. Gao, Q. Wang, X. Gao, C. Ding, and D. Tao, "Tensorized bipartite graph learning for multi-view clustering," *IEEE Transactions on Pattern Analysis and Machine Intelligence*, vol. 45, no. 4, pp. 5187–5202, 2022.
- [42] F. Nie, X. Wang, and H. Huang, "Clustering and projected clustering with adaptive neighbors," in *Proceedings of the 20th ACM SIGKDD international conference on Knowledge discovery and data mining*, 2014, pp. 977–986.
- [43] R. Chakraborty and B. C. Vemuri, "Statistics on the stiefel manifold: theory and applications," 2019.
- [44] M. E. Kilmer, K. Braman, N. Hao, and R. C. Hoover, "Third-order tensors as operators on matrices: A theoretical and computational framework with applications in imaging," *SIAM Journal on Matrix Analysis and Applications*, vol. 34, no. 1, pp. 148–172, 2013.
- [45] Z. Kang, G. Shi, S. Huang, W. Chen, X. Pu, J. T. Zhou, and Z. Xu, "Multi-graph fusion for multi-view spectral clustering," *Knowledge-Based Systems*, vol. 189, p. 105102, 2020.
- [46] Z. Ren, S. X. Yang, Q. Sun, and T. Wang, "Consensus affinity graph learning for multiple kernel clustering," *IEEE Transactions on Cybernetics*, vol. 51, no. 6, pp. 3273–3284, 2020.
- [47] Y. Chen, X. Xiao, and Y. Zhou, "Jointly learning kernel representation tensor and affinity matrix for multi-view clustering," *IEEE Transactions on Multimedia*, vol. 22, no. 8, pp. 1985–1997, 2019.

- [48] H. Wang, G. Han, B. Zhang, G. Tao, and H. Cai, "Multi-view learning a decomposable affinity matrix via tensor self-representation on grassmann manifold," *IEEE Transactions on Image Processing*, vol. 30, pp. 8396–8409, 2021.
- [49] J. Chen, G. Han, H. Cai, J. Ma, M. Kim, P. Laurienti, and G. Wu, "Estimating common harmonic waves of brain networks on stiefel manifold," in *Medical Image Computing and Computer Assisted Intervention–MICCAI 2020: 23rd International Conference, Lima, Peru, October 4–8, 2020, Proceedings, Part VII 23*. Springer, 2020, pp. 367–376.
- [50] S. Boyd, N. Parikh, E. Chu, B. Peleato, J. Eckstein *et al.*, "Distributed optimization and statistical learning via the alternating direction method of multipliers," *Foundations and Trends® in Machine learning*, vol. 3, no. 1, pp. 1–122, 2011.
- [51] S. P. Boyd and L. Vandenberghe, *Convex optimization*. Cambridge university press, 2004.
- [52] W. Hu, D. Tao, W. Zhang, Y. Xie, and Y. Yang, "The twist tensor nuclear norm for video completion," *IEEE transactions on neural networks and learning systems*, vol. 28, no. 12, pp. 2961–2973, 2016.
- [53] K. Zhan, F. Nie, J. Wang, and Y. Yang, "Multiview consensus graph clustering," *IEEE Transactions on Image Processing*, vol. 28, no. 3, pp. 1261–1270, 2018.
- [54] M.-S. Chen, L. Huang, C.-D. Wang, and D. Huang, "Multi-view clustering in latent embedding space," in *Proceedings of the AAAI conference on artificial intelligence*, vol. 34, no. 04, 2020, pp. 3513–3520.
- [55] W. Xia, X. Zhang, Q. Gao, X. Shu, J. Han, and X. Gao, "Multiview subspace clustering by an enhanced tensor nuclear norm," *IEEE Transactions on cybernetics*, vol. 52, no. 9, pp. 8962–8975, 2021.
- [56] S.-G. Fang, D. Huang, X.-S. Cai, C.-D. Wang, C. He, and Y. Tang, "Efficient multi-view clustering via unified and discrete bipartite graph learning," *IEEE Transactions on Neural Networks and Learning Systems*, 2023.
- [57] Y. Tan, Y. Liu, H. Wu, J. Lv, and S. Huang, "Metric multi-view graph clustering," in *Proceedings of the AAAI Conference on Artificial Intelligence*, vol. 37, no. 8, 2023, pp. 9962–9970.
- [58] Y. Tan, Y. Liu, S. Huang, W. Feng, and J. Lv, "Sample-level multi-view graph clustering," in *Proceedings of the IEEE/CVF Conference on Computer Vision and Pattern Recognition*, 2023, pp. 23 966–23 975.